Journal of Non-Crystalline Solids 536 (2020) 119995

Contents lists available at ScienceDirect

Journal of Non-Crystalline Solids

journal homepage: www.elsevier.com/locate/jnoncrysol

Amorphous silicon triboride: A first principles study

Ayşegül Özlem Çetin Karacaoğlan, Murat Durandurdu*

Materials Science and Nanotechnology Engineering and Materials Science & Mechanical Engineering Program, Abdullah Gül University, Kayseri, Turkey

ARTICLE INFO

Keywords:
Amorphous
Silicon triboride
Electronic structure
Mechanical properties

ABSTRACT

Using *ab initio* molecular dynamics simulations, an amorphous silicon triboride (a-SiB_3) network is generated and its atomic structure, electronic features and mechanical properties are compared with those of the crystal. The average coordination number of B and Si atoms in a-SiB_3 is found as 5.8 and 4.6, correspondingly, close to 6.0 (B atom) and 5.0 (Si atom) in the crystal. A careful investigation reveals partial structural similarities around B atoms but not around Si atoms in both phases of SiB_3. The presence of B_{12}, $B_{11}Si$ and B_{10} molecules is witnessed in a-SiB_3. The last two molecules, however, do not exist in the crystal. a-SiB_3 is a semiconducting material. The bulk modulus of the ordered and disordered structures is projected to be 151 GPa and 131 GPa, respectively. The Vickers hardness of a-SiB_3 is calculated to be ~13–15 GPa, less than ~20–25 GPa estimated for the crystal.

1. Introduction

Boron (B), a III-A group element, is a trivalent metalloid showing both metal and non-metal characteristics and has drawn considerable attention due to its unique/complex structures and properties [1]. B can have a rich variety of compounds [1] and form a strong covalent bond with other elements because of sp^2 hybridization and its small radius [2,3]. B compounds such as BN, BC, BO, BMg, and BSi are extensively used as engineering materials for various purposes more than a century because of their interesting and unusual properties [4,5,6]. Among these compounds, silicon borides or boron silicides (BSi) have drawn considerable attention on superconductivity in the thermoelectric devices [4,5,7,8].

Moissan and Stock performed the first original study on BSi systems in 1900 [9] and were able to prepare two different crystalline borides, silicon triboride (c-SiB_3) and silicon hexaboride (c-SiB_6), by fusion of the elements. In 1955, Samsonov and Latysheva were able to fabricate the c-SiB_3 single phase by means of the hot pressing at temperatures of 1873–2073 K [10]. According to Samsonov and Latysheva's study [10], c-SiB_3 was available if the samples contained between 21 mol% and 27 mol% of Si. The invariant reaction for the SiB_3 crystal was also reported in the literature [11,12]. In a different study, β-SiB_3 was proposed as the alternative orthorhombic phase of SiB_3 [13].

Noncrystalline SiB materials having a wide range of B and Si concentrations were synthesized using different experimental protocols [14,15,16,17,18,19]. Amorphous B_xSi_{1-x} ($0 \leq x \leq 1$) systems were produced by radio frequency (rf) plasma decomposition of silane-diborane gas mixtures [14]. Si-rich amorphous SiB binary compounds having B content ranging from 0 to 40% at various temperatures between 25–700 °C [15] and from 1% to 50% at temperatures of 400–520 °C were fabricated by low pressure chemical vapor deposition (LPCVD) method [16]. Besides, amorphous BSi films with Si/B atomic ratios of 1/9, 2/8, 3/7, 4/6 and 5/5 were manufactured by pulsed laser deposition process [17]. B-rich SiB materials having B concentration in the range of 90.0–97.0% were synthesized by arc-melting and spark plasma sintering protocol [18]. As expected, the optical band gap of B-rich amorphous SiB materials increases with decreasing B content [17]. It appears that when B concentration is higher, the oxidation of Si and B components in the amorphous SiB alloys is faster in compared to both Si and B crystals [19].

Boron rich amorphous SiB systems have suitable properties such as high hardness and high-temperature stability and hence are expected to have applications as high-temperature thermoelectric materials [14,20]. However, a clear atomistic level description of these alloys is not available in the literature. In order to better understand these materials, perhaps as a first step, the amorphous form of the SiB crystals should be modelled and compared with its crystalline counterpart whose the structure and properties are known. To our knowledge, the amorphous state of SiB_3 (a-SiB_3) has not been investigated so far. The aim of the present work is to determine the microstructure and the mechanical and electrical features of a-SiB_3, to associate them with those of the crystal and to make some contributions to the literature. In particular, we would like reveal whether the amorphous state is as useful as the crystal and offers some practical applications in technology.

* Corresponding author.
E-mail address: murat.durandurdu@agu.edu.tr (M. Durandurdu).

https://doi.org/10.1016/j.jnoncrysol.2020.119995
Received 9 December 2019; Received in revised form 7 February 2020; Accepted 24 February 2020

2. Computational method

The molecular dynamics (MD) calculations were achieved by the SIESTA ab initio code [21] that is based on the density functional theory (DFT). The pseudopotentials were established by the Troullier–Martins scheme [22]. The double zeta basis set was chosen for the valence electrons and the Γ point was used for the Brillion zone integration. The exchange correlation energy was due to the PBE-GGA method [23]. The isothermal-isobaric (NPT) ensemble was constituted to perform the MD simulations. Each MD time was set to 1.0 fs. The temperature applied was controlled by the velocity scaling and the volume of the supercell at ambient pressure was adjusted by the Parrinello–Rahman technique [24] having a fictitious mass of 20.0 Ry.fs^2. Our simulation box had randomly distributed 200 atoms (150 B atoms and 50 Si atoms) and its initial density was 2.0219 g/cm^3. The supercell was subjected to a temperature of 2000 K for around 40 ps. The density of the system increased to a value of 2.2198 g/cm^3 in less than 5.0 ps and it fluctuated slightly between 2.1717 and 2.2198 g/cm^3 in the rest of the simulation time at 2000 K. The melt was then slowly quenched to 300 K by using a cooling rate of 2.0 × 10^{12}*K/s*. At room temperature, it was additionally equilibrated for 2.0 ps and the resulting structure was optimized using a conjugate gradient method. For the optimization, the force criterion was set to be 0.02 eV/Å. The density of the relaxed amorphous phase was 2.2941 g/cm^3, which is marginally less than 2.4341 g/cm^3 predicted for the crystal, as expected because most amorphous states have a lower density than their crystalline counterparts. Our value for the crystal is slightly less than the experimental prediction of 2.47 g/cm^3 [25] and the theoretical value of 2.45 g/cm^3 [26] based on a plane wave calculation.

3. Results

3.1. Atomic structure

The microstructure of the ordered and disordered SiB_3 phases illustrated in Fig. 1 is firstly compared by the partial pair distribution function (PPDF) analysis given in Fig. 2. The first neighbor B-B separation of the amorphous model is located at 1.76 Å that is fairly close to 1.77 Å in the crystal. Additionally, this value is comparable with experimental result of 1.78 Å reported for amorphous B [27]. The second peak of the B-B correlation is positioned at 2.97 Å, which is again objectively parallel to 2.95 Å in the crystal and 3.02 Å in amorphous B [27]. Consequently, based on these results, we can propose that the distribution of B-atoms in the noncrystalline state is comparable with that of B-atoms in the crystal and even in amorphous B. The first two peaks of B-Si pair of a-SiB_3 are at 2.04 Å and 3.34 Å, respectively. They are again analogous to 1.99 Å and 3.34 Å in the crystalline phase. Our B-Si distance is also akin to the experimental values of 1.89–1.94 Å reported for the Si_3B crystal [28]. The Si-Si bond distance is estimated to be 2.38 Å for a-SiB_3 and 2.57 Å for c-SiB_3. So, an obvious decrease in the Si-Si bond separation is perceived by amorphization, which might be the indication of the formation of different type of Si motifs in both phases.

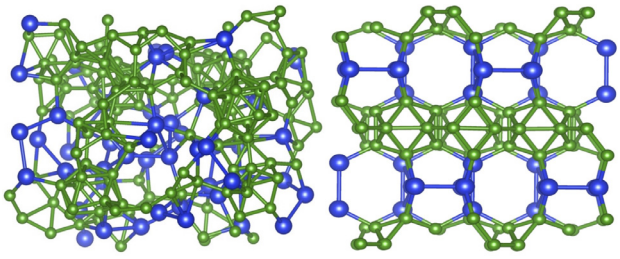

(a) (b)

Fig. 1. (a) Amorphous and (b) crystalline forms of SiB_3.

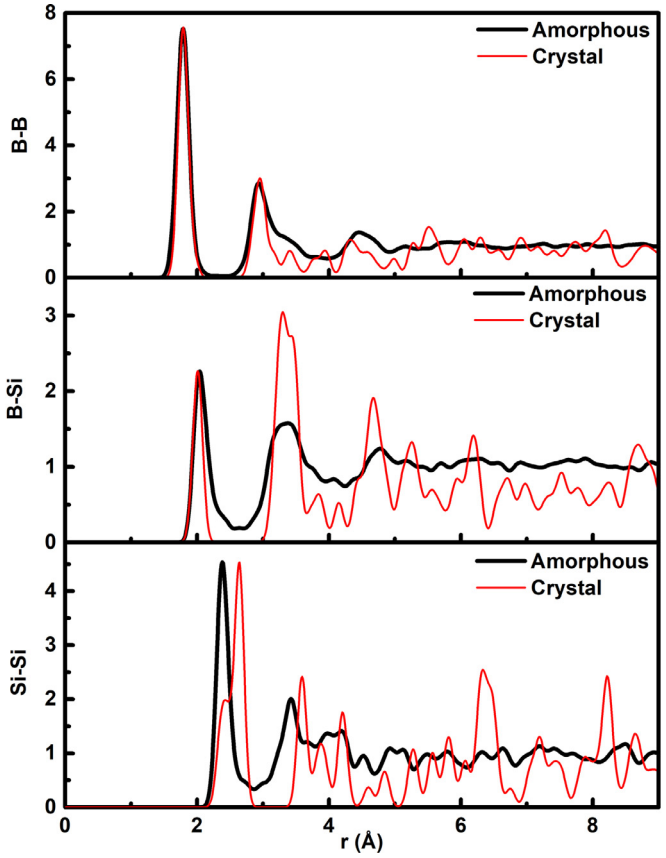

Fig. 2. Partial pair correlation functions (PPDFs) of c-SiB_3 and a-SiB_3, which are plotted using Gaussian smoothing factor of 0.05. Also, to clearly compare both structures, the intensity of PPDFs of the crystal is scaled.

In order to determine the type of configurations formed in the short-range order of both phases, we estimate their partial coordination numbers using the first minimum (B-B = 2.35 Å, B-Si = 2.62 Å, Si-Si = 2.88 Å for the amorphous and B-B = 2.37 Å, B-Si = 2.62 Å, Si-Si = 2.78 Å for the crystal) of the PPDFs. The mean coordination number of B and Si atoms in the amorphous state is found as 5.8 and 4.6, respectively, which are very close to 6.0 (B atoms) and 5.0 (Si atoms) in the crystal. As shown in the Fig. 3, the most common unit for B atoms is sixfold-coordination with a frequency of about 61%. The fraction of fivefold- and sevenfold-coordination for B atoms is 20.7% and 12.7%, correspondingly. On the other hand, the most privileged motif for Si atoms is fourfold-coordination having a frequency of 52%. Si atoms present a nonnegligible amount of fivefold-(24%) and sixfold-(20%) coordination as well. Accordingly, one can see here that Si atoms have a tendency to form fourfold instead of fivefold coordination.

The coordination analysis provides useful information at the atomistic level but does not offer a depth understanding of the local structure of the amorphous network. Such an understanding can be attainable by the chemical environmental analysis. Table 1 presents the chemical distribution of each species. According to the Table, B-B_6 (27.33%) and B-B_5Si (26.67%) type of clusters are the key units around B atoms in a-SiB_3. Indeed, they are the main building motifs of the crystal having frequencies of 33.33% and 66.67%, respectively. In addition to them, a visible number of B-B_7, B-B_3Si_2 and B-B_4Si motifs is perceived in the amorphous configuration. Thus, it can be concluded here that the formation of B-B_5Si is less favorable in the amorphous state than in the crystal and approximately 50% of B atoms in the noncrystalline network have the arrangements, analogous to those of the crystal. For Si atoms, Si-BSi_3 (24%) and Si-B_2Si_2 (16%) units are found as the most dominated ones in the a-SiB_3 model. Besides, Si-

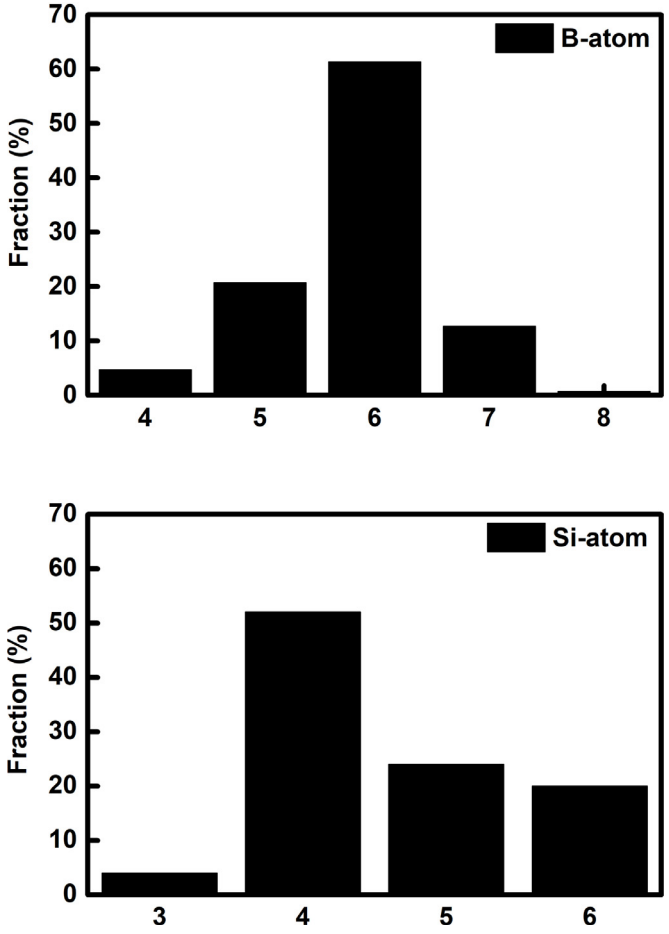

Fig. 3. Coordination distribution in a-SiB_3.

Table 1
Chemical distribution in a-SiB_3. CN is the coordination number.

CN	B atom		CN	Si atom	
3	B_2Si	0.67%	3	B_2Si	2.00%
4	B_3Si	2.00%	4	BSi_3	24.00%
4	B_4	1.33%	4	B_2Si_2	16.00%
4	Si_4	0.67%	4	B_3Si	2.00%
5	BSi_4	1.33%	4	B_4	4.00%
5	B_2Si_3	1.33%	5	BSi_4	2.00%
5	B_3Si_2	8.67%	5	B_2Si_3	4.00%
5	B_4Si	8.00%	5	B_3Si_2	10.00%
5	B_5	2.00%	5	B_4Si	8.00%
6	B_3Si_3	2.00%	5	B_5	2.00%
6	B_4Si_2	5.33%	5	Si_5	2.00%
6	B_5Si	26.67%	6	B_3Si_3	8.00%
6	B_6	27.33%	6	B_4Si_2	6.00%
7	B_6Si	2.00%	6	B_5Si	2.00%
7	B_7	10.00%	6	B_6	2.00%
8	B_7Si	0.67%	7	B_3Si_4	2.00%
			7	B_5Si_2	4.00%

B_3Si_2, Si-B_3Si_3, Si-B_4Si and Si-B_4Si_2 type of structures having a low fraction are also presented in the disordered structure. On the other hand, c-SiB_3 consists of only Si-B_2Si_3 type of motif and such a motif does indeed barely exist in the amorphous network, implying that the chemical environment of Si atoms in a-SiB_3 does not coincide with that of c-SiB_3. On the basis of these findings, one can conclude here that although the average coordination of a-SiB_3 is comparable with that of the crystal, its local structure marginally resembles to that of the crystal.

In order to reveal similarities/distinctions between two phases in details, we perform the Voronoi polyhedral investigation. The cutoff radii used in the coordination and chemical distribution analyses are adopted for this investigation as well. A Voronoi polyhedron, a three dimensional solid figure having many plane faces, is symbolized by indices $\langle l_3, l_4, l_5, l_6, \ldots\rangle$ where l_i represents the number of i-edge faces of a polyhedron and $\Sigma\, l_i$ is its total coordination number. In the crystal, B atoms form just one type of cluster represented by $\langle 2,2,2,0\rangle$ index, which is the pentagonal pyramid-like unit. In the amorphous state, B atoms structure largely in the $\langle 2,2,2,0\rangle$ type of configuration with a fraction of 59% as well. Additionally, an incomplete pentagonal pyramid-like unit having $\langle 2,3,0,0\rangle$ (19%) index appear in the amorphous phase. Consequently, most B-atoms form a polyhedron similar to one formed in the crystal. On the other hand, Si atoms create only $\langle 2,3,0,0\rangle$ type polyhedron in the crystal while they construct the $\langle 2,2,2,0\rangle$ (20%), $\langle 2,3,0,0\rangle$ (22%) and $\langle 4,0,0,0\rangle$ (46%) kind of arrangements in the amorphous network. So, tetrahedral configuration appears to be the dominated one for Si atoms. Perhaps, the most interesting finding is the presence of a nonnegligible amount the pentagonal pyramid-like units $\langle 2,2,2,0\rangle$ around Si-atoms in the amorphous state. A close analysis reveals that the pentagonal pyramid-like configurations of B and Si atoms lead to the formation of the B_{12}, $B_{11}Si$ and B_{10} molecules (see Fig. 4) in the noncrystalline state. It should be noted that last two molecules are not presented in the crystal.

Bond angle distribution examination given in Fig. 5 might provide extra information about the model at the atomistic level. The analysis exposes apparent differences between two forms of SiB_3 considering their atomic structure. The most noticeable difference is the presence of a broad Si-B-Si distribution in a-SiB_3 contrary to the crystalline state. The B-B-B distribution has two principal peaks at around 60° and 107° for both amorphous and crystal structures. These angles are due to the intraicosahedral bonds of the pentagonal pyramids (B_{12} icosahedrons). The B-Si-B angles for the amorphous model produce a broad distribution changing from 40° to 150°, quite different than sole angle of around 117° in the crystal. It should be noted that this distribution is someway similar to that of the B-B-B angles since some Si atoms have a trend to create the pentagonal pyramid-like structures. The amorphous system has a wide Si-Si-Si angle distribution ranging from 50° to 150° while the crystalline phase has three peaks at 60°, 90° and 120°. All these findings support only partial similarities, particularly around B atoms, in both phases of SiB_3.

3.2. Electrical properties

c-SiB_3 is a semiconducting material having a GGA band gap of about 1.4 eV [26]. In order to see how amorphization affects on the electronic structure of SiB_3 and to uncover if the amorphous form can serve as an electronic material, we study its electron density of states (EDOS) and partial electron density of states (PDOS) and compare them with those of the crsytal. The EDOS of the amorphous and crystalline phases is depicted in Fig. 6. According to the EDOS analysis, both structures exhibit a semiconducting behavior. The HOMO-LUMO band gap energy of the amorphous and crystalline states is found to be 0.2 eV and 1.86 eV (that is slightly higher than the GGA result of 1.4 eV [26]),

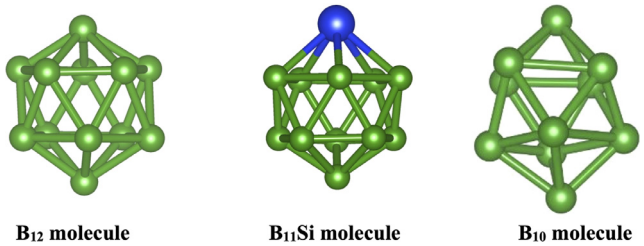

Fig. 4. B_{12}, $B_{11}Si$ and B_{10} molecules formed in a-SiB_3.

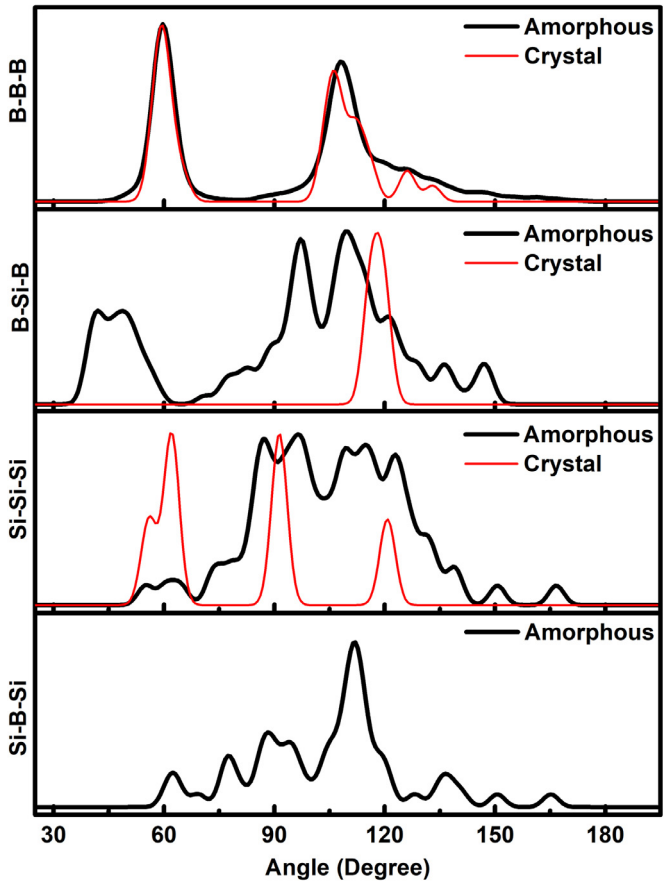

Fig. 5. Bond angle distribution of a-SiB_3 and c-SiB_3.

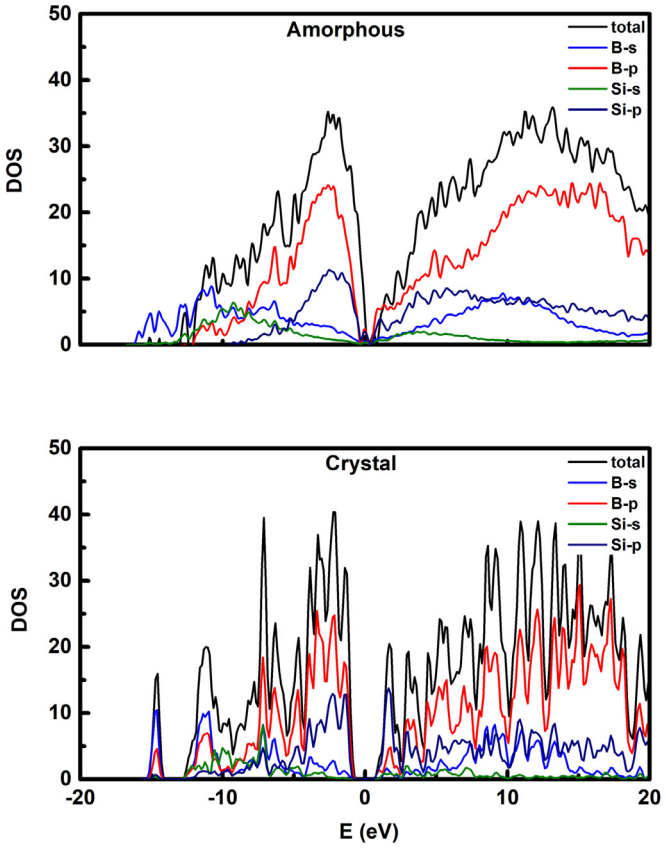

Fig. 6. Total and partial electron density of states.

correspondingly. The gap value predicted for amorphous phase appears to be reasonable considering the experimental values of 0.5–0.75 eV reported for B-rich amorphous BSi materials [17] in spite of underestimation of the band gap in DFT-GGA simulations. PDOS given in Fig. 6 can offer more information regarding the electronic structure. Fig. 6 reveals that the most dominant states for both conduction and valence bands are B-*p* electrons, similar to what has been reported in the earlier study [29], while the other states have a minimal effect to the bands near the Fermi level.

3.3. Mechanical properties

The practical applications of a material commonly require the knowledge on its mechanical properties. In this section we study the mechanical properties of both structures of SiB_3 and compare them in details. Firstly, we focus on the bulk modulus (K) which can be easily estimated by fitting the energy (E)-volume (V) relation of the amorphous and crystalline phases (Fig. 7) to the third-order Birch-Murnaghan equation of states,

$$E(V) = E_0 + \frac{9V_0K}{16}\left\{\left[\left(\frac{V_0}{V}\right)^{\frac{2}{3}} - 1\right]^3 K' + \left[\left(\frac{V_0}{V}\right)^{\frac{2}{3}} - 1\right]^2\left[6 - 4\left(\frac{V_0}{V}\right)^{\frac{2}{3}}\right]\right\}$$

where the subscript "0" refers the equilibrium values and $K' = dK/dP$ and P is pressure. The K value is found to be ~131 GPa for the amorphous network and ~159 GPa for the crystal. Consequently, a slight decrease in bulk modulus is experienced in SiB_3 by amorphization, which is anticipated because of the disordered nature of a-SiB_3. Our K value is found to be comparable with 171.2 GPa estimated for c-SiB_3 [29].

In order to estimate Young's modulus (E), defined as the resistance

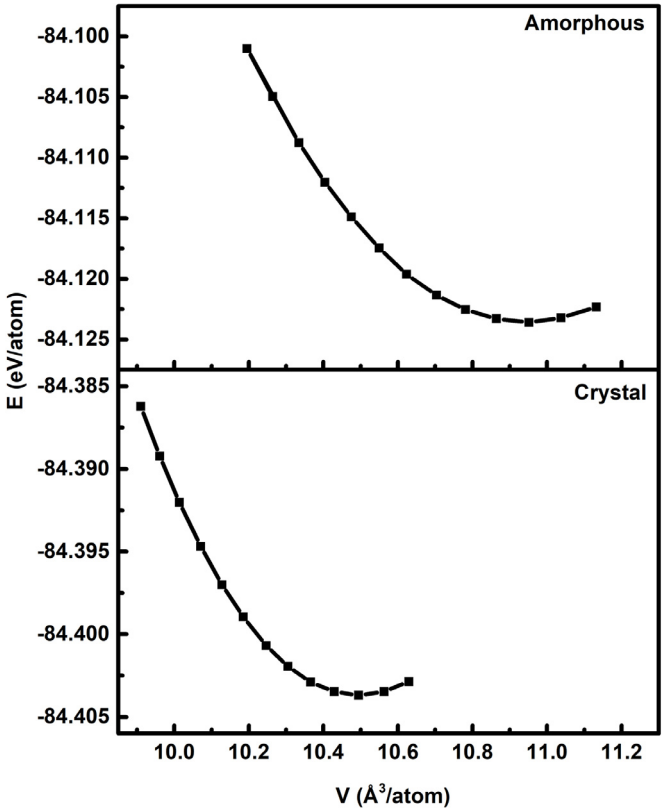

Fig. 7. Energy as a function of volume.

of a material to elastic deformation under loading, a uniaxial stress is applied along the principle axes (*x, y* and *z*) of the SiB_3 phases while the other stress components are set to be zero. Both the simulation cell parameters and the atomic coordinates are permitted to relax. From the stress (σ) – strain (Ɛ) relation;

$$E = \frac{\sigma_{axial}}{\varepsilon_{axial}}$$

the average E is calculated as 310.8 GPa for the crystal and 211.8 GPa for the amorphous network. The Young modulus of the amorphous phase is noticeably smaller than the crystal meaning that the amorphous form is more elastic than the crystal. We should point out here that our value for c-SiB_3 precisely overlaps with the earlier theoretical prediction [29].

Using the following definition,

$$\nu = \frac{1}{2} - \frac{E}{6K}$$

the Poisson ratio is projected to be as 0.23 for the amorphous phase and 0.17 for the crystal, close to the earlier estimation of 0.2 [29].

We calculate shear modulus (μ), the modulus of rigidity, representing the resistance to plastic deformation,

$$\mu = \frac{E}{2(1+\nu)}$$

to be around 86 GPa for a-SiB_3 and 132.4 GPa for the crystal, comparable with the previous theoretical result of 129.8 GPa [29]. Note that the smaller μ value of the amorphous form indicates that it is more flexible than the crystal.

By using three different equations [30,31,32]

$$H = 0.151\mu$$

$$H = 2\left(\frac{\mu}{n^2}\right)^{0.585} - 3(GPa)$$

and

$$H = 0.92\left(\frac{1}{n}\right)^{1.137}\cdot(\mu)^{0.708}$$

the Vickers hardness is predicted to be 13.3–14.2 GPa for the amorphous state and 20–25 GPa for the crystal. So, one can see that amorphization leads to a substantial decrease in the Vickers hardness.

From the Pugh's ratio ($n = K/\mu$), it is possible to predict the brittle or ductile behavior of a material. 1.75 is accepted as a critical value for n. If n is bigger than 1.75, the material is classified as a ductile solid. If n is smaller than 1.75, it is classified as a brittle solid. n is calculated as 1.53 for a-SiB_3 and 1.2 for c-SiB_3. Subsequently, both phases present a brittle character but the amorphous form will show better performance of resistance to stress cracking than the crystal since the higher Pugh's ratio means less brittleness.

4. Conclusions

The microstructure, electronic structure and mechanical features of an a-SiB_3 network created using ab *initio* MD calculations are compared with those of the crystalline phase. In the amorphous state, Si and B atoms have the mean coordination numbers of 5.8 and 4.6, correspondingly, comparable with 6.0 (B atom) and 5.0 (Si atom) in the crystal. The local structure of a-SiB_3 is found to be partially parallel to that of the crystal. Specifically, partial structural similarities around B atoms are observed in both phases of SiB_3. However, such similarities are not detected around Si-atoms. The occurrence of B_{12}, $B_{11}Si$ and B_{10} molecules is observed in a-SiB_3 but the last two do not form in the crystal. a-SiB_3 presents a semiconducting behavior but its energy band gap is noticeably less than that of the crystal. The bulk modulus is projected to be 131 GPa for the amorphous configuration and 159 GPa for the crystalline state. The Vickers hardness of a-SiB_3 is calculated to be around 13–15 GPa, less than 20–25 GPa estimated for the crystal. So amorphization significantly influences the atomic structure, electronic properties and mechanical features of SiB_3. Yet, different preparation techniques such as irradiation, mechanical milling, and high pressure (some B rich materials can transform to amorphous state at high pressure) might lead to an amorphous network with a distinct local structure and of course the distinct microstructure may result in different electrical and mechanical properties. Therefore, additionally studies using different preparation protocols are needed to better understand a-SiB_3.

CRediT authorship contribution statement

Ayşegül Özlem Çetin Karacaoğlan: Investigation, Validation, Formal analysis, Data curation, Writing - original draft, Visualization. **Murat Durandurdu:** Conceptualization, Methodology, Resources, Supervision, Funding acquisition, Writing - review & editing.

Declaration of Competing Interest

The authors declare that they have no known competing financial interests or personal relationships that could have appeared to influence the work reported in this paper.

Acknowledgements

This work was supported by the Scientific and Technological Research Council of Turkey(TÜBİTAK) under grant number 117M372. AÖÇK would like to acknowledge partial support by YÖK 100/2000 and TÜBİTAK BİDEB 2211-C programs. The simulations were run on the TÜBİTAK High Performance and Grid Computing Center (TRUBA resources).

Supplementary materials

Supplementary material associated with this article can be found, in the online version, at doi:10.1016/j.jnoncrysol.2020.119995.

References

[1] B. Albert, Boron: elementary challenge for experimenters and theoreticians, Angew. Chem. Int. Ed. 48 (2009) 8640–8668.
[2] L. Cheng, B14: an all-boron fullerene, J. Chem. Phys. 136 (2012) 104301-104301.
[3] N.G. Szwacki, A. Sadrzadeh, B.I. Yakobson, B80 fullerene: an ab initio prediction of geometry, stability, and electronic structure, Phys. Rev. Lett. 98 (2007) 166804-166804.
[4] M. Mukaida, T. Tsunoda, Y. Imai, Preparation of B-Si films by chemical vapor deposition, Proc. 18th Int. Conf. Thermoelectrics. (1999) 667–670.
[5] T.B. Tai, P. Kadłuban´ski, S. Roszak, D. Majumdar, J. Leszczynski, M.T. Nguyen, Electronic structures and thermochemical properties of the small silicon-doped boron clusters BnSi (n = 1–7) and their anions, Chem. Phys. Chem. 12 (2011) 2948–2958.
[6] G.L. Perkins, Boron: compounds, production, and application, Nova Science Pub. Inc. (2011).
[7] J. Wang, G. Sun, P. Kong, W. Sun, C. Lu, F. Peng, X. Kuang, Novel structural phases and the electrical properties of Si_3B under high pressure, Phys. Chem. Chem. Phys. 19 (2017) 16206–16212.
[8] M. Vlasse, G.A. Slack, M. Garbauskas, J.S. Kasper, J.C. Viala, The crystal structure of SiB_6, j, Solid State Chem. 63 (1986) 31–45.
[9] H. Moissan, A. Stock, Preparation and properties of two silicon borides: SiB_3 and SiB_6, C.R. Acad Sci. 131 (1900) 139–143.
[10] G.V. Samsonov, V.P. Latysheva, Chemical compounds of boron with silicon, Dokl. Akad. Nauk SSSR 105 (1955) 499-499.
[11] J. Wu, W. Ma, D. Tang, B. Jia, B. Yang, D. Liu, Y. Dai, Thermodynamic description of Si-B binary system, Procedia Eng. 31 (2012) 297–301.
[12] R.W. Cahn, Binary alloy phase diagrams, Adv. Mater. 3 (1991) 628–629.
[13] J.R. Salvador, D. Bilc, S.D. Mahanti, Stabilization of beta-SiB3 from liquid Ga: a boron-rich binary semiconductor resistant to high-temperature air oxidation, Angew Chem 42 (2003) 1929–1932.
[14] C.C. Tsai, Characterization of amorphous semiconducting silicon-boron alloys prepared by plasma decomposition, Phys. Rev. B 19 (1979) 2041–2055.
[15] W.M. Lau, R. Yang, B.Y. Tong, S.K. Wong, Thermal oxidation of amorphous silicon-boron alloy, MRS Online Proc. Lib. Arch. 105 (1987) 163–167.

[16] G.R. Yang, Y.P. Zhao, B.Y Tong, Studying low-pressure chemical vapor deposition a-Si:B alloys by optical spectroscopy, J. Vac. Sci. Technol. A: Vacuum Surfaces Films 16 (1998) 2267–2271.
[17] M. Takeda, M. Ichimurai H. Yamaguchi, Y. Sakairi, K. Kimura, Preparation of boron–silicon thin film by pulsed laser deposition and its properties, J. Solid State Chem. 154 (2000) 141–144.
[18] L. Chen, T. Goto, J. Li, T. Hirai, Synthesis and thermoelectric properties of boron-rich silicon borides, Mater. Trans. JIM. 37 (1996) 1182–1185.
[19] G.R. Yang, Y.P. Zhao, M. Abburi, S. Dabral, B.Y. Tong, Comparison of low-temperature oxidation of crystalline Si and B with a-Si:B alloy: an x-ray photoelectron spectroscopy study, J. Vac. Sci. Technol. A: Vacuum, Surfaces Films 15 (1997) 279–283.
[20] B. Armas, G. Male, D. Salanoubat, C. Chatillon, M. Allibert, Determination of the boron-rich side of the B-Si phase diagram, J. Less Common Met. 82 (1981) 245–254.
[21] P. Ordejón, E. Artacho, J.M. Soler, Self-consistent order-N density-functional calculations for very large systems, Phys. Rev. B. 53 (1996) R10441–R10444.
[22] N. Troullier, J.M. Martins, Efficient pseudopotentials for plane-wave calculations, Phys. Rev. B. 43 (1991) 1993–2006.
[23] J.P. Perdew, K. Burke, M Ernzerhof, Generalized gradient approximation made simple, Phys. Rev. Lett. 77 (1996) 3865–3868.
[24] M. Parrinello, A. Rahman, Polymorphic transitions in single crystals: a new molecular dynamics method, J. Appl. Phys. 52 (1981) 7182–7190.
[25] D. Eklöf, A. Fischer, A. Ektarawong, A. Jaworski, A.J. Pell, J. Grins, S.I. Simak, B. Alling, Y. Wu, M. Widom, W. Scherer, U. Häussermann, Mysterious SiB_3: identifying the relation between α- and β-SiB3, ACS Omega 4 (2019) 18741–18759.
[26] https://materialsproject.org/.
[27] R.G. Delaplane, T. Lundstrom, U. Dahlborg, W.S. Howells, D. Emin, T.L. Aselage, A.C. Switendick, B. Morosin, C.L. Beckel (Eds.), Boron-Rich Solids, 231 AIP Conf, Proc, 1991, pp. 241–244.
[28] R. Viswanathan, R.W. Schmude, K.A. Gingerich, Thermochemistry of BSi (g), BSi2 (g), and BSi3 (g), J. Phys. Chem. 100 (1996) 10784–10786.
[29] B. Zhang, L. Wu, Z. Li, Predicted structural evolution and detailed insight into configuration correlation, mechanical properties of silicon–boron binary compounds, RSC Adv. 7 (2017) 16109–16118.
[30] D.M. Teter, Computational alchemy: the search for new superhard materials, Mrs Bull. 23 (1998) 22–27.
[31] X.Q. Chen, H. Niu, D. Li, Y. Li, Modeling hardness of polycrystalline materials and bulk metallic glasses, Intermetallics 19 (2011) 1275–1281.
[32] Y. Tian, B. Xu, Z. Zhao, Microscopic theory of hardness and design of novel superhard crystals, Int. J. Refract. Met. H. 33 (2012) 93–106.